Parametrizations of inclusive cross sections for pion production in proton-proton collisions

Steve R. Blattnig, Sudha R. Swaminathan, Adam T. Kruger, Moussa Ngom, and John W. Norbury
Physics Department, University of Wisconsin-Milwaukee, P.O. Box 413, Milwaukee, Wisconsin 53201
(Received 17 February 2000; revised manuscript received 30 May 2000; published 12 October 2000)

Accurate knowledge of cross sections for pion production in proton-proton collisions finds wide application in particle physics, astrophysics, cosmic ray physics, and space radiation problems, especially in situations where an incident proton is transported through some medium, and one requires knowledge of the output particle spectrum given the input spectrum. In such cases accurate parametrizations of the cross sections are desired. In this paper we review much of the experimental data and compare it with a wide variety of different cross section parametrizations. In so doing, we provide parametrizations of neutral and charged pion cross sections which provide a very accurate description of the experimental data. Lorentz invariant differential cross sections, spectral distributions, and total cross section parametrizations are presented.

PACS number(s): 13.85.Ni

I. INTRODUCTION

Pion production in proton-proton collisions has been extensively studied over many years, and has now reached the point where this knowledge finds useful applications in a variety of areas, as detailed below.

(1) Two important types of particle detectors are the hadronic and electromagnetic calorimeters [1], in which an electromagnetic or hadronic shower is initiated by a high energy incoming particle. From a Monte Carlo simulation of the shower, one is able to deduce important characteristics of the incoming particle such as its energy and identity.

(2) The primary cosmic rays can be detected by a variety of methods, depending on the incident energy. For the very high energy cosmic rays, where the flux is relatively low, the extensive air showers (EAS's) [2–4] provide the most convenient means of detection. The EAS is analogous to the hadronic or electromagnetic calorimeter used in particle physics, but with the Earth's atmosphere being the active volume in which the shower develops. The EAS has both electromagnetic and hadronic components, and similar to the calorimeter, the energy and identity of primary cosmic ray nuclei can be deduced via Monte Carlo simulation of the showers [2,3].

(3) In long duration human space flights, such as a mission to Mars, the radiation levels induced by galactic cosmic rays can exceed exposure limits set for astronauts [5,6]. In determining the radiation environment inside a spacecraft one needs to transport the exterior cosmic ray spectrum through the spacecraft wall in order to determine the interior radiation spectrum.

(4) In γ-ray [7,8] and high energy neutrino astronomy [9,10], the diffuse background radiation is due in large part to the γ rays and neutrinos produced in proton collisions with the protons in the interstellar medium. In addition, pion production from proton-proton collisions finds applications in the calculation of γ-ray emission from the accretion disk around a black hole [11].

In all of the above applications it is crucial to have an accurate knowledge of the cross sections for pion production in proton-proton collisions. In addition, most of the applications mentioned above require solving the transport equations which determine the particle spectrum on one side of a material (active volume of calorimeter, Earth's atmosphere, spacecraft wall, or interstellar medium) given the incident particle spectrum. Use of pion production cross sections in such transport codes requires that the cross section be written in a simple form. The transport codes have many iterative loops, which will take too much computer time if the cross section formulas also contain many iterative loops. Thus it is most advantageous if one can write down simple formulas which parametrize all of the experimental data on pion production cross sections. That is the aim of the present work.

In this paper we provide simple algebraic parametrizations of charged and neutral pion production cross sections valid over a range of energies. The cross sections we provide are Lorentz-invariant differential cross sections (LIDCS's), lab frame spectral distributions (i.e., energy differential cross sections), and total cross sections, because these are the types of cross sections most widely used in transport equations. Many authors have presented such parametrizations before, but the problem is to decide which authors are correct and whether a particular parametrization applies only to a limited data set or is valid over a wider range. In the present work, we have performed an exhaustive data search and have compared as many different parametrizations as possible to as much data as possible, so as to provide definitive conclusions as to which is the most accurate parametrization to use. All of this is discussed more extensively below.

The cross sections discussed in this paper are for inclusive pion production in proton-proton collisions, i.e., the reactions considered are $p+p \rightarrow \pi + X$, where p represents a proton, π represents a pion, and X represents any combination of particles. An extensive search for LIDCS data was performed, and the data were used to compare all available parametrizations. An extensive set of data was used in these comparisons, but only a few data points are graphed in this paper due to space considerations. A method for generating parametrizations for these cross sections is also described and applied to π^0 production. Spectral distribution and total cross section formulas were not developed directly because of a lack of data. Instead, the most successful LIDCS parametrizations were first transformed into lab frame spectral distributions by numerical integration. These cross sections were also param-

etrized. Finally, the total cross sections were compared to available data and parametrized as well. This procedure is discussed, and the parametrizations of the numerical results are given. Multiple checks of the accuracy of all results were made, and some of these are presented.

Notation. Starred quantities (e.g., θ^*) refer to the quantities in the center of mass (c.m.) frame, while unstarred quantities (e.g., θ) refer to the quantities in the lab frame.

$E(d^3\sigma/d^3p) \equiv$ Lorentz-invariant differential cross section (LIDCS)

$d\sigma/dE \equiv$ spectral distribution $= 2\pi p \int_0^{\theta_{\max}} d\theta\, E(d^3\sigma/d^3p)\sin\theta$

$\sigma \equiv$ total cross section $= 2\pi \int_0^{\theta_{\max}} d\theta \int_{p_{\min}}^{p_{\max}} dp\, E(d^3\sigma/d^3p) \times (p^2 \sin\theta/\sqrt{p^2+m_\pi^2}) = \int_{E_{\min}}^{E_{\max}} (d\sigma/dE)dE$

P_p is the proton momentum.

m_p is the proton mass.

m_π is the pion mass.

$\sqrt{s}$ is the magnitude of the total four momentum, and is equal to the total energy in the c.m. frame.

$T_{\rm lab}$ is the lab frame kinetic energy of the incoming proton.

T is the pion kinetic energy.

E is the pion total energy.

θ is the angle of pion scattering with respect to the direction of the incident particle.

p is the pion momentum.

$p_\perp \equiv p_t$ is the pion transverse momentum ($p_\perp = p \sin\theta$).

$p_{\max}$ is the maximum possible momentum the scattered pion can have for a given $\sqrt{s}$.

II. COMPARISON OF LORENTZ INVARIANT DIFFERENTIAL CROSS SECTIONS

The object has been to determine an accurate parametrization for inclusive LIDCS, which can be confidently applied to regions where no experimental data are available. For example, the parametric equation would need to be extrapolated to energies lower than those for which data are available, if the formulas were to be used for the purpose of developing radiation shielding materials. The most convenient formulas are those that are in closed form, since they are easily used, and take relatively little CPU time in numerical calculations. Some of the formulas that were considered as representations of the LIDCS were not in closed form, but included tabulated functions of energy (i.e., numerical values were given for specific energy values rather than a functional form). When comparing parametrizations, closed form expressions were given precedence over other equally accurate formulas.

The invariant single-particle distribution is defined by

$$f(AB\to CX) \equiv E_c \frac{d^3\sigma}{d^3p_c} \equiv E\frac{d^3\sigma}{d^3p} = \frac{E}{p^2}\frac{d^3\sigma}{dp\,d\Omega}, \qquad (1)$$

where $d^3\sigma/d^3p_c$ is the differential cross section (i.e., the probability per unit incident flux) for detecting a particle C within the phase-space volume element d^3p_c. A and B are the initial colliding particles, C is the produced particle of interest, and X represents all other particles produced in the collision. E is the total energy of the produced particle C, and Ω is the solid angle. This form is favored since the quantity is invariant under Lorentz transformations.

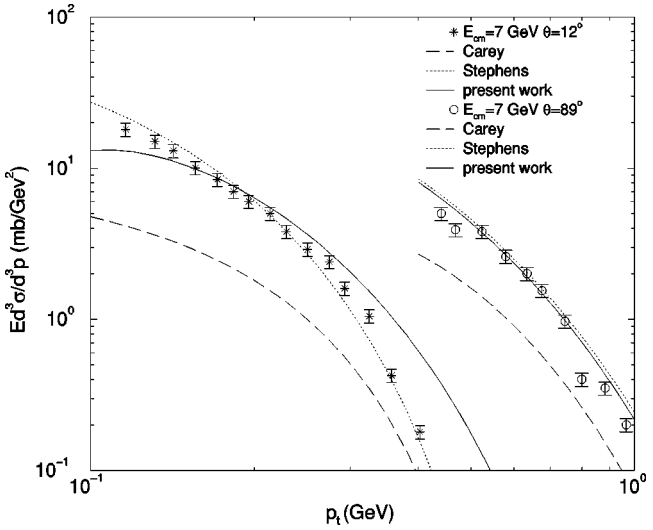

FIG. 1. π^0 production parametrizations of Carey *et al.* [Eq. (5)] [15], of Stephens and Badhwar [Eq. (6)] [20], and of Eq. (7) plotted with LIDCS data from [14,20]. LIDCS is plotted against transverse momentum for c.m. energy $E_{\rm c.m.}=7$ GeV. The pion c.m. scattering angle is $12.2<\theta^*<12.4°$ and $\theta^*=89°$ for the data, and the parametrizations are plotted at $\theta^*=12°$ and $\theta^*=89°$.

The data for pion production in proton-proton interactions are primarily reported in terms of the kinematic variables $\theta^*, \sqrt{s}, p_\perp$, which are, respectively, the c.o.m. frame scattering angle of the pion, the invariant mass of the entire system, and the transverse momentum of the produced pion. $\sqrt{s}$ is a Lorentz invariant quantity, and is equal to the total energy in the c.o.m. frame. $p_\perp \equiv p^* \sin\theta^*$, where p^* is the c.o.m. momentum. $p_\perp$ is invariant under the transformation from the lab frame to the c.m. frame. (See [12] for a more detailed discussion of kinematic variables.) In the following discussions, all momenta, energies, and masses are in units of GeV.

A. Neutral pions

Busser *et al.* [13] have fitted the LIDCS data obtained in the reaction $p+p\to\pi^0+X$, where p represents a proton, π^0 represents the neutral pion produced, and X represents all other produced particles, to an equation of the form

$$E\frac{d^3\sigma}{d^3p} = Ap_\perp^{-n}\exp\left(-b\frac{p_\perp}{\sqrt{s}}\right), \qquad (2)$$

with $A=1.54\times10^{-26}$, $n=8.24$, and $b=26.1$. This equation is based on a specific set of experimental data with all measurements taken at $\theta^*\simeq90°$, and was originally intended only for pions with high $p_\perp$. Comparison of this parametrization with data available from other experiments [14–20] indicates that the global behavior of the invariant cross section cannot be represented by a function of this form. See Figs. 1–3 for some examples of data. The parametrization of

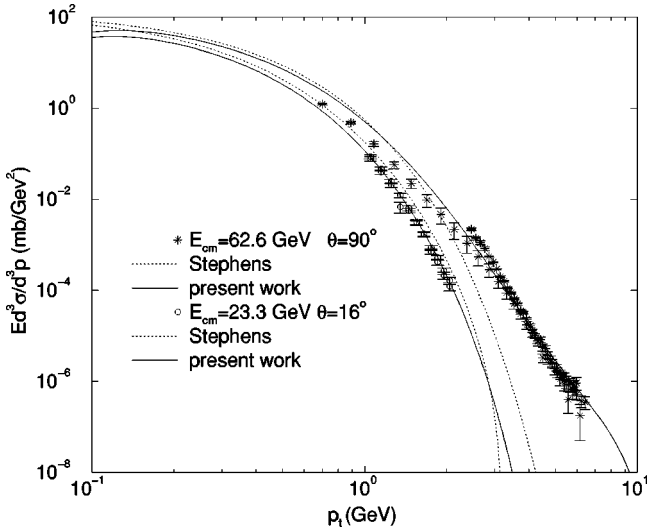

FIG. 2. π^0 production parametrizations of Carey *et al.* [Eq. (5)] [15], of Stephens and Badhwar [Eq. (6)] [20], and of Eq. (7) plotted with LIDCS data from [13,16,17]. The first set of data is for c.m. energy $E_{\text{c.m.}}=62.4$ and 62.9 GeV at c.m. scattering angle $\theta^*=90°$ and the parametrizations are plotted at $E_{\text{c.m.}}=62.6$ GeV at $\theta^*=90°$. The second set of data is at c.m. energy $E_{\text{c.m.}}=23.3$ GeV and the pion c.m. scattering angle $\theta^*=15°$ and 17.5° for the data, and the parametrizations are plotted at $\theta^*=16°$.

Busser *et al.* [13] was not plotted because the cross section is much too small compared to the data in the $p_\perp$ ranges covered by the graphs.

The following form has been used by Albrecht *et al.* [21] to represent neutral pion production:

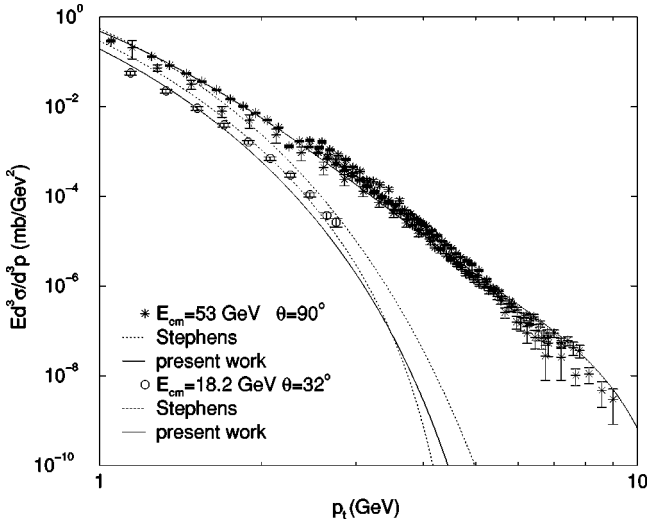

FIG. 3. π^0 production parametrizations of Carey *et al.* [Eq. (5)] [15], of Stephens and Badhwar [Eq. (6)] [20], and of Eq. (7) plotted with LIDCS data from [15]. For the first set of data, LIDCS is plotted against transverse momentum for c.m. energy $E_{\text{c.m.}}=18.2$ GeV. The pion c.m. scattering angle $32.3°<\theta^*<32.5°$ for the data, and the parametrizations are plotted at $\theta^*=32°$. The second set of data and parametrizations are at $E_{\text{c.m.}}=53$ GeV, $\theta^*=90°$. The data are from [13,16–18].

$$E\frac{d^3\sigma}{d^3p}=C\left(\frac{p_0}{p_\perp+p_0}\right)^n, \tag{3}$$

where C, n, and p_0 are free parameters. This equation only has dependence on $p_\perp$ where as the data [14–20], some of which is shown in Figs. 1–3, also have dependence on $\sqrt{s}$ and θ^*. This form is therefore not general enough to represent all the data.

Ellis and Stroynowski [22] have favored a representation for the invariant cross section of the form

$$E\frac{d^3\sigma}{d^3p}=A(p_\perp^2+M^2)^{-N/2}f(x_\perp,\theta^*) \tag{4}$$

where $f(x_\perp,\theta^*)=(1-x_\perp)^F$, N and F are free parameters, and the scaling variable $x_\perp$ is given by $x_\perp=p_\perp/p^*_{\max}\simeq 2p_\perp/\sqrt{s}$. $p^*_{\max}=[(s+m_\pi^2-4m_p^2)^2/4s-m_\pi^2]^{1/2}$, where m_π and m_p are the mass of the neutral pion and the proton, respectively, is the maximum pion momentum allowed. The outline of this basic form has been used by Carey *et al.* in fitting the invariant cross section for the inclusive reaction $p+p\rightarrow\pi^\circ+X$ [23]. Their representation is given by

$$E\frac{d^3\sigma}{d^3p}=A(p_\perp^2+0.86)^{-4.5}(1-x_R^*)^4, \tag{5}$$

where $x_R^*=p^*/p^*_{\max}$ is the radial scaling variable and the normalization constant A has been determined as $A\simeq 5$. This parametrization accurately reproduces the data for measurements taken at $\theta^*=90°$ and $\sqrt{s}\geq 9.8$ GeV, but does not agree well with the data for lower energies ($\sqrt{s}=7$ GeV). The disagreement at lower energies can be seen in Fig. 1.

Another problem with this parametrization becomes apparent when one considers that integration over all allowed angles and outgoing particle momenta should yield the total inclusive cross section. The details of this calculation appear in Sec. III. A comparison of the experimentally determined total cross section data from Whitmore [24] with the results of the numerical integration of Eq. (5) shows that the total cross section is greatly underestimated by Carey. See Fig. 4.

Stephens and Badhwar [20] obtained data from the photon cross sections given by Fidecaro [14]. The Fidecaro data were taken at incident proton kinetic energy $T_{\text{lab}}=23$ GeV and $p_\perp=0.1-1.0$ GeV. (Note: No error was listed by Fidecaro *et al.* [14] for pion production. Error bars of 10% were added to the data on the figures, since this level of error was standard for most of the other data. Also, Stephens uses the notation E_p instead of T_{lab}.) Figures 1–3 show common examples of the accuracy of Badhwar and Stephens' parametrization's fit to the data. The following is the parametrization of the π^0 invariant cross section proposed by Stephens and Badhwar [20]:

$$E\frac{d^3\sigma}{d^3p}=Af(T_{\text{lab}})(1-\tilde{x})^q\exp(-Bp_\perp/(1+4m_p^2/s)), \tag{6}$$

where

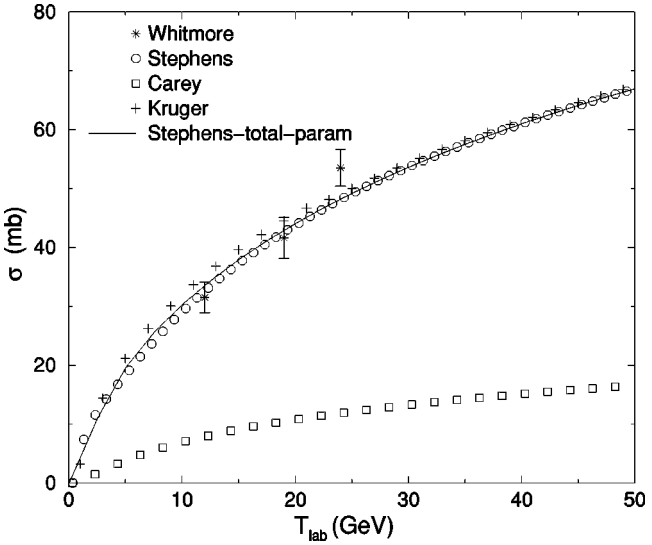

FIG. 4. Parametrization of total π^0 production cross section plotted with *numerically integrated* LIDCS parametrizations of Stephens and Bodhwar [Eq. (6)] [20], of Carey *et al.* [Eq. (5)] [15], and of Eq. (7) referred to as Kruger. The curve labeled ''Stephens-total-param'' is the parametrization given in Eq. (29). Three data points from Whitmore [24] are included for comparison.

$$\tilde{x} = \sqrt{\left\{ (x_\parallel^*)^2 + \left(\frac{4}{s}\right)(p_\perp^2 + m_\pi^2) \right\}},$$

$$q = \frac{C_1 - C_2 p_\perp + C_3 p_\perp^2}{\sqrt{1 + 4m_p^2/s}},$$

$$f(T_{\rm lab}) = (1 + 23 T_{\rm lab}^{-2.6})(1 - 4m_p^2/s)^2$$

and

$$A = 140,\ B = 5.43,\ C_1 = 6.1,\ C_2 = 3.3,\ C_3 = 0.6,$$

$$\text{with } x_\parallel^* \equiv p_\parallel^*/p_{\rm max}^*, \text{ and } p_\parallel^* = p^* \cos\theta^*.$$

The Stephens-Badhwar parametrization was found to be the best of the previously listed representations, because it accurately reproduces the data in the low $p_\perp$ region, where the cross section is greatest (see Figs. 1–3), and its integration yields accurate values for the total cross section (see Fig. 4). This equation is, however, a poor tool for predicting values of the invariant cross section for $p_\perp \gtrsim 3$ GeV, where the value predicted underestimates experimental data by up to $\simeq$10 orders of magnitude (see Figs. 2 and 3).

No parametrization currently exists that accurately fits the global behavior of the LIDCS data. Previous equations have suffered from being too specific to a particular set of experimental data, or from failing to reproduce the total cross section upon integration. It is for these reasons that a new parametrization is desired, one that correctly predicts all available data while maintaining the essential quality of correctly producing the total cross section upon integration.

The approach that has been adopted in the present work is to assume the following form for the invariant cross section:

$$E\frac{d^3\sigma}{d^3p} = (\sin\theta^*)^{D(\sqrt{s},p_\perp,\theta^*)} F(\sqrt{s},p_\perp,\theta^* = 90°). \quad (7)$$

The motivation for an equation of this form is that as the angle decreases, the cross section decreases very slowly at lower $p_\perp$ values. The approximation that was made in deriving the above equation is that as $p_\perp \to 0$, the cross section is assumed to be independent of angle.

Under the assumption that the invariant cross section can be fitted by Eq. (7), the program goes as follows. Find a representation for the cross section as a function of energy $\sqrt{s}$ and transverse momentum $p_\perp$ from experimental data taken at $\theta^* = 90°$. $F(\sqrt{s},p_\perp)$ is then completely determined, because $(\sin\theta^*)^D$ is unity at $\theta^* = 90°$.

At $\theta^* = 90°$ the data are well represented by

$$E\frac{d^3\sigma}{d^3p}(\theta^* = 90°) \equiv F(\sqrt{s},p_\perp),$$

with

$$F(\sqrt{s},p_\perp) = \ln\left(\frac{\sqrt{s}}{\sqrt{s}_{\rm min}}\right) G(q,p_\perp), \quad (8)$$

where $q = s^{1/4}$ and the c.m. pion production threshold energy $\sqrt{s}_{\rm min} = 2m_p + m_\pi$. The function

$$G(q,p_\perp) \equiv \frac{E\frac{d^3\sigma}{d^3p}(\theta^* = 90°)}{\ln\left(\frac{\sqrt{s}}{\sqrt{s}_{\rm min}}\right)}$$

was parametrized as

$$\begin{aligned} G(q,p_\perp) = \exp\{ & k_1 + k_2 p_\perp + k_3 q^{-1} + k_4 p_\perp^2 + k_5 q^{-2} \\ & + k_6 p_\perp q^{-1} + k_7 p_\perp^3 + k_8 q^{-3} \\ & + k_9 p_\perp q^{-2} + k_{10} p_\perp^2 q^{-1} + k_{11} p_\perp^{-3} \}, \end{aligned} \quad (9)$$

with $k_1 = 3.24$, $k_2 = -6.046$, $k_3 = 4.35$, $k_4 = 0.883$, $k_5 = -4.08$, $k_6 = -3.05$, $k_7 = -0.0347$, $k_8 = 3.046$, $k_9 = 4.098$, $k_{10} = -1.152$, and $k_{11} = -0.0005$. The parameters $k_1 - k_{10}$ were obtained using the numerical curve fitting software Table Curve 3D v3 [26] and the eleventh term was added to modify the low $p_\perp$ behavior of the parametrization.

With $F(\sqrt{s},p_\perp)$ determined, the function $D(\sqrt{s},p_\perp,\theta^*)$ is the only remaining unknown. Solving for D yields

$$D(\sqrt{s},p_\perp,\theta^*) = \frac{\ln\left(E\frac{d^3\sigma}{d^3p}\right) - \ln(F(\sqrt{s},p_\perp))}{\ln(\sin\theta^*)}. \quad (10)$$

Equations (8) and (9) were then used in Eq. (10) to calculate values of $D(\sqrt{s},p_\perp,\theta^*)$. If the function D is independent of angle, then Eq. (10) could be determined for any fixed angle, $\theta^* \neq 90°$. Data were compared for a range of angular values, and this data revealed that the function D is

not independent of the angle. The angular dependence turned out to be of the form $(\sin\theta^*)^{-0.45}$ and

$$D(\sqrt{s},p_\perp,\theta^*)=(\sin\theta^*)^{-0.45}\times\left[c_1 p_\perp^{c_2}(\sqrt{s})^{c_3}+c_4\frac{p_\perp}{\sqrt{s}}+\frac{c_5}{\sqrt{s}}+\frac{1.0}{s}\right] \tag{11}$$

with $c_1=205.7$, $c_2=3.308$, $c_3=-2.875$, $c_4=10.43$, and $c_5=0.8$.

The final form of our resultant parametrization for the neutral pion invariant cross section in proton-proton collisions is Eq. (7) with $F(p_\perp,\sqrt{s})$ given in Eq. (8), $G(q,p_\perp)$ given in Eq. (9), and $D(p_\perp,\sqrt{s},\theta^*)$ given in Eq. (11). This form is accurate over a much greater range of transverse momentum values than those covered by previous representations. Figures 1–3 show a few comparisons. A much more extensive set of data was used in the development and comparison of the parametrizations, but they are not shown in this paper due to space considerations. For the low transverse momentum region where the cross section is the greatest, the fit is quite similar to that of Stephens and Badhwar [20]. Also, Fig. 4 shows that both formulas (6 and 7) integrate to approximately the same total cross section, which is in agreement with the data from Whitmore [24]. [Equation (7) integrated into a total cross section is denoted as Kruger in Fig. 4.] A more complete comparison of the integrated total cross section to the data is given by Stephens and Badhwar [20]. Note however that Eq. (7) was based mainly on the data from [14–20]. Equation (7) could therefore given unpredictable results in regions not included in those data sets, particularly for very low transverse momentum or $\sqrt{s}\gg 63\,\mathrm{GeV}$.

B. Charged pions

The available data for charged pions, is less extensive than π^0 data. There is therefore a higher degree of uncertainty in LIDCS for charged pions. Integration of a LIDCS to get a total cross section and comparison of the results to total cross section data, allows a check of the global fit of a parametrization. This check was made for charged as well as neutral pions, but due to a lack of data, it is more important for charged pions. Parametrizations that do not integrate to the correct total cross section can be ruled out, even if the LIDCS data are well represented, because the global behavior of the parametrization cannot be accurate. However, producing a correct total cross section upon integration does not necessarily imply that the global behavior of the parametrization is correct. A tighter constraint could be placed on possible LIDCS parametrizations, if more measurements were made. If the spectral distribution is measured at three different values of pion energy for two different proton collision energies, the general behavior of the spectral distribution could be determined. The angular dependence of LIDCS parametrization could then be tested by integrating over the angle, and comparing the results to the spectral distribution data. For the purposes of space radiation shielding, measurements at proton lab kinetic energies of 3 and 6 GeV, and pion lab kinetic energies of 0.01, 0.1, and 1 GeV would be useful, because this is the region with both a large cross section, and large galactic cosmic ray fluxes. With these facts in mind, a comparison of LIDCS parametrizations with data from [16,25,27–29] for charged pion production follows. A parametrization for π^- of the form

$$E\frac{d^3\sigma}{d^3p}=A\exp(-Bp_\perp^2) \tag{12}$$

has been given by Albrow *et al.* [29] where A and B are tabulated functions of $x_R^*\equiv p^*/p^*_{\max}$. A and B are given only for $x_R^*=0.18$, $x_R^*=0.21$, and $x_R^*=0.25$, which limits the usefulness of this parametrization.

Alper *et al.* [25] have fitted the data for both π^+ and π^- production to the following form:

$$E\frac{d^3\sigma}{d^3p}=A\exp(-Bp_\perp+Cp_\perp^2)\exp(-Dy^2), \tag{13}$$

where y is the longitudinal rapidity, and A, B, C, and D are tabulated functions of s, that are also dependent on the type of produced particle (π^+ or π^-). (Note that at $\theta^*=90°$ we have $y=0$.) The fit to the data is excellent for low transverse momentum, as can be seen in Figs. 8 and 10, but these figures also show that this form has an increasing cross section for high $p_\perp$, which contradicts the trend in the data. Also, there are different sets of constants for each different energy, which makes a generalization to arbitrary energies difficult.

Parametrizations done by Carey *et al.* [30] and Ellis and Stroynowski [22] have a similar form, although Carey's was applied only to π^-. Both underestimate LIDCS for low $p_\perp$, where the cross section is the largest (see Figs. 7–10).

The following is Carey's parametrization:

$$E\frac{d^3\sigma}{d^3p}(\pi^-)=N(p_\perp^2+0.86)^{-4.5}(1-x_R^*)^4, \tag{14}$$

where $N=13$ is the overall normalization constant, and $x_R^*\equiv p^*/p^*_{\max}\approx 2p^*/\sqrt{s}$.

The following is Ellis's parametrization which was applied to both π^+ and π^- production at $\theta^*=90°$:

$$E\frac{d^3\sigma}{d^3p}=A(p_\perp^2+M^2)^{-N/2}(1-x_\perp)^F, \tag{15}$$

where M,N,F are given constants. A is an unspecified overall normalization for which we used $A=13$, and $x_\perp\equiv p_\perp/p^*_{\max}\approx 2p_\perp/\sqrt{s}$.

The most successful LIDCS parametrization available for charged pion production was found to be the one developed by Badhwar *et al.* [31]

$$E\frac{d^3\sigma}{d^3p}=\frac{A(1-\tilde{x})^q}{(1+4m_p^2/s)^r}e^{[-Bp_\perp/(1+4m_p^2/s)]}, \tag{16}$$

where q is a function of $p_\perp$, and s, such that

$$q=(C_1+C_2p_\perp+C_3p_\perp^2)/(1+4m_p^2/s)^{1/2}$$

and

$$\tilde{x}\approx\left[x_\parallel^{*2}+\frac{4}{s}(p_\perp^2+m_\pi^2)\right]^{1/2}.$$

Here $x_\parallel^*=p_\parallel^*/p_{\max}^*\approx 2p_\parallel^*/\sqrt{s}$. For π^+, $A=153$, $B=5.55$, $C_1=5.3667$, $C_2=-3.5$, $C_3=0.8334$, and $r=1$. For π^-, $A=127$, $B=5.3$, $C_1=7.0334$, $C_2=-4.5$, $C_3=1.667$, and $r=3$. This form is accurate for low transverse momentum (Figs. 7–12), which is the most important region for radiation shielding due to the large cross section. It is also in closed form, so that extra numerical complexities do not have to be considered. A comparison to a few data points, shown in Fig. 13, demonstrates that it integrates to the correct total cross section. A more detailed comparison of the integrated cross section to experimental data is given by Badhwar *et al.* [31]. Because of its relative accuracy and simplicity, this parametrization was integrated to get total cross sections and spectral distributions for charged pions.

Mokhov and Striganov [32] have also developed the following formulas for both π^+ and π^- production:

$$E\frac{d^3\sigma}{d^3p}=A\left(1-\frac{p^*}{p_{\max}^*}\right)^B\exp\left(-\frac{p^*}{C\sqrt{s}}\right)V_1(p_\perp)V_2(p_\perp), \tag{17}$$

where

$$V_1=(1-D)\exp(-Ep_\perp^2)+D\exp(-Fp_\perp^2)$$

$$\text{for } p_\perp\leqslant 0.933\,\text{GeV}$$

$$=\frac{0.2625}{(p_\perp^2+0.87)^4}\quad\text{for } p_\perp>0.933\,\text{GeV}$$

and

$$V_2=0.7363\exp(0.875p_\perp)\quad\text{for } p_\perp\leqslant 0.35\,\text{GeV}$$

$$=1\quad\text{for } p_\perp>0.35\,\text{GeV},$$

with $A=60.1$, $B=1.9$, and $C=0.18$ for π^+, $A=51.2$, $B=2.6$, and $C=0.17$ for π^-, and $D=0.3$, $E=12$, and $F=2.7$ for both π^+ and π^-. Figures 7–12 show that the formula of Badhwar has a better fit to the data in the low $p_\perp$ region where the cross section is the largest.

III. SPECTRAL DISTRIBUTIONS AND TOTAL CROSS SECTIONS

A. Method of generating other cross sections from a LIDCS

While LIDCS's contain all the necessary information for a particular process, sometimes other cross sections are needed. For example, one dimensional radiation transport requires probability density distributions that are integrated over the solid angle. These quantities are calculated in terms of spectral distributions and total cross sections rather than LIDCS, but with accurate parametrizations of LIDCS, formulas for both spectral distributions and total cross sections can be developed. LIDCS for inclusive pion production in proton-proton collisions contain dependence on the energy of the colliding protons ($\sqrt{s}$), on the energy of the produced pion (T_π), and on the scattering angle of the pion (θ). Total cross sections σ, which depend only on $\sqrt{s}$, and spectral distributions $d\sigma/dE$, which depend on $\sqrt{s}$ and T_π, can be extracted from a LIDCS by integration. If azimuthal symmetry is assumed, these cross sections take the following form:

$$\frac{d\sigma}{dE}=2\pi p\int_0^{\theta_{\max}}d\theta\,E\frac{d^3\sigma}{d^3p}\sin\theta, \tag{18}$$

$$\sigma=2\pi\int_0^{\theta_{\max}}d\theta\int_{p_{\min}}^{p_{\max}}dp\,E\frac{d^3\sigma}{d^3p}\frac{p^2\sin\theta}{\sqrt{p^2+m_\pi^2}}, \tag{19}$$

where $\theta_{\max}$, $p_{\max}$, and $p_{\min}$ are the extrema of the scattering angle and momentum of the pion, respectively, and m_π is the rest mass of the pion.

In the c.m. frame these extrema can easily be determined. Using conservation of momentum and energy, one can easily show that

$$p^2=\frac{(s+m_\pi^2-s_x)^2}{4s}-m_\pi^2, \tag{20}$$

where s_x is the square of the invariant mass of the sum of all particles excluding the pion, and p is the magnitude of the three momentum of the pion. The independence of p on θ implies that θ can take on all possible values (i.e., $\theta_{\max}=\pi$), and the symmetry of the c.m. frame implies that $p_{\min}=0$. For a given value of s, it is obvious that momentum is a maximum when s_x is a minimum. An invariant mass is a minimum, when it is equal to the square of the sum of the rest masses of the particles in question. Momentum is, therefore, a maximum when s_x is the square of the sum of the least massive combination of particles that can be produced while still satisfying all relevant conservation laws. For the reaction $p+p\rightarrow\pi+x$, we have $s_x\simeq 4m_p^2$, where the subscript p represents a proton.

If a Lorentz transformation is applied to the maximum c.m. momentum, the integration limits can be determined in other frames. Byckling and Kajantie have shown that by transforming to the lab frame, the following formula can be obtained [12]:

$$p_\pi^\pm=[p_aE_{\max}^*\sqrt{s}\cos\theta\pm(E_a+m_p)\sqrt{sp_{\max}^{*2}-m_\pi^2p_a^2\sin^2\theta}]\times[s+p_a^2\sin^2(\theta)]^{-1}, \tag{21}$$

where starred quantities are c.m. variables, and unstarred quantities are either lab or invariant variables, m_p is the rest mass of a proton; p_a is the magnitude of the momentum of the projectile proton, and $p^+=p_{\max}$ is the maximum pion momentum. The greater of the two quantities $p^-=p_{\min}$ and 0 is the minimum pion momentum, and the maximum scattering angle can be determined by the requirement that $p^\pm$ be

TABLE I. Constants for Eq. (23).

$A_1=6.78\times10^{-10}$	$A_8=-1.75$	$A_{15}=0.25$
$A_2=-2.86$	$A_9=-32.1$	$A_{16}=-39.4$
$A_3=1.82\times10^{-8}$	$A_{10}=0.0938$	$A_{17}=2.88$
$A_4=-1.92$	$A_{11}=-23.7$	$A_{18}=0.025$
$A_5=22.3$	$A_{12}=0.0313$	$A_{19}=0.75$
$A_6=0.226$	$A_{13}=2.5\times10^{6}$	
$A_7=-0.33$	$A_{14}=1.38$	

TABLE II. Constants for Eq. (24).

$B_1=1.3\times10^{-10}$	$B_8=-1.25$	$B_{15}=60322$
$B_2=-2.86$	$B_9=-33.2$	$B_{16}=1.07$
$B_3=4.27\times10^{-9}$	$B_{10}=0.0938$	$B_{17}=-67.5$
$B_4=-2.4$	$B_{11}=-23.6$	
$B_5=22.3$	$B_{12}=0.0313$	
$B_6=-1.87$	$B_{13}=2.5\times10^{6}$	
$B_7=1.28$	$B_{14}=0.25$	

real. This requirement implies that the quantity under the square root must be greater than or equal to 0. Solving for $\theta_{\max}$ then gives the formula

$$\theta_{\max}=\sin^{-1}\left(\frac{\sqrt{s}p^*_{\max}}{p_a m_\pi}\right). \tag{22}$$

With the limits of integration determined, a LIDCS can be turned into a total cross section or a spectral distribution by numerical integration. This procedure will, however, give discrete ''data'' points; not closed form expressions. Parametrizations of this numerical data are needed, if relatively simple formulas for these cross sections are desired. This process was completed for all three pion species, and the corresponding formulas are listed in Sec. III B. It should be noted that the accuracy of these parametrizations is limited to that of the original LIDCS.

B. Parametrizations

The surface parametrizations for the spectral distribution as a function of incident proton kinetic energy in the lab frame $T_{\rm lab}$ and the lab kinetic energy of the produced pion T_π have been completed by numerically integrating LIDCS charged pion parametrizations due to Badhwar *et al.* [Eq. (16)] [31] and the neutral pion cross section both from Stephens and Badhwar [Eq. (6)] [20], and from Eq. (7). The numerical integration routines were checked for accuracy by computing total cross sections in both the lab and c.m. frames and comparing the results. Since total cross section is invariant under the transformation between these two frames, the results should be the same in both frames. In order to accurately fit the integration points for low energies, it has been necessary to consider two regions of the surface and to determine representations for them individually. For each of the three pions, the two regions consist of laboratory kinetic energies $T_{\rm lab}$ from 0.3 to 2 GeV and from 2 to 50 GeV. Using the following parametrizations in energy regions other than the region listed above could give unpredictable results since the formulas were not tested there.

The neutral pion spectral distribution for the range 0.3–2 GeV is represented by the following equations:

$$F_2=A_1T_\pi^{A_2}+A_3T_{\rm lab}^{A_4},$$

$$F_1=\exp\left(A_5+\frac{A_6}{\sqrt{T_{\rm lab}}}+A_7T_{\rm lab}^{A_8}+A_9T_\pi^{A_{10}}+A_{11}T_\pi^{A_{12}}\right), \tag{23}$$

$$\left(\frac{d\sigma}{dE}\right)_{\rm lab}=\left(A_{13}\frac{F_1}{F_2}+A_{14}\exp(A_{16}\sqrt{T_\pi}+A_{17}T_\pi^{A_{18}}T_{\rm lab}^{A_{19}})\right)T_\pi^{A_{15}},$$

with constants A_i given in Table I.

The neutral pion spectral distribution for the range 2–50 GeV is represented by the following equations:

$$F_2=B_1T_\pi^{B_2}+B_3T_{\rm lab}^{B_4},$$

$$F_1=\exp\left(B_5+\frac{B_6}{\sqrt{T_{\rm lab}}}+B_7T_{\rm lab}^{B_8}+B_9T_\pi^{B_{10}}+B_{11}T_\pi^{B_{12}}\right), \tag{24}$$

$$\left(\frac{d\sigma}{dE}\right)_{\rm lab}=B_{13}T_\pi^{B_{14}}\frac{F_1}{F_2}+B_{15}T_\pi^{B_{16}}\exp(B_{17}\sqrt{T}_\pi),$$

with constants B_i given in Table II.

The positively charged pion spectral distribution for the range 0.3–2 GeV is represented by the following equations:

$$F_2=C_1T_\pi^{C_2}+C_3T_{\rm lab}^{C_4},$$

$$F_1=\exp\left(C_5+\frac{C_6}{\sqrt{T_{\rm lab}}}+C_7T_{\rm lab}^{C_8}+C_9T_\pi^{C_{10}}+C_{11}T_\pi^{C_{12}}T_{\rm lab}^{C_{13}}+C_{14}\ln T_{\rm lab}\right), \tag{25}$$

$$\left(\frac{d\sigma}{dE}\right)_{\rm lab}=C_{15}T_\pi^{C_{16}}\frac{F_1}{F_2}+C_{17}T_\pi^{C_{18}}\exp(C_{19}\sqrt{T_\pi}+C_{20}\sqrt{T_{\rm lab}}),$$

with constants C_i given in Table III.

The positively charged pion spectral distribution for the range 2–50 GeV is represented by the following equations:

TABLE III. Constants for Eq. (25).

$C_1=2.2\times10^{-8}$	$C_8=-1.75$	$C_{15}=2.5\times10^{6}$
$C_2=-2.7$	$C_9=-29.4$	$C_{16}=0.25$
$C_3=4.22\times10^{-7}$	$C_{10}=0.0938$	$C_{17}=976$
$C_4=-1.88$	$C_{11}=-24.4$	$C_{18}=2.3$
$C_5=22.3$	$C_{12}=0.0312$	$C_{19}=-46$
$C_6=1.98$	$C_{13}=0.0389$	$C_{20}=-0.989$
$C_7=-0.28$	$C_{14}=1.78$	

TABLE IV. Constants for Eq. (26).

$D_1=4.5\times10^{-11}$	$D_7=-35.3$	$D_{13}=60322$
$D_2=-2.98$	$D_8=0.0938$	$D_{14}=1.18$
$D_3=1.18\times10^{-9}$	$D_9=-22.5$	$D_{15}=-72.2$
$D_4=-2.55$	$D_{10}=0.0313$	$D_{16}=0.941$
$D_5=22.3$	$D_{11}=2.5\times10^{6}$	$D_{17}=0.1$
$D_6=-0.765$	$D_{12}=0.25$	

$$F_2=D_1T_\pi^{D_2}+D_3T_{\rm lab}^{D_4},$$

$$F_1=\exp\left(D_5+\frac{D_6}{\sqrt{T_{\rm lab}}}+D_7T_\pi^{D_8}+D_9T_\pi^{D_{10}}\right), \tag{26}$$

$$\left(\frac{d\sigma}{dE}\right)_{\rm lab}=D_{11}T_\pi^{D_{12}}\frac{F_1}{F_2}+D_{13}T_\pi^{D_{14}}\exp(D_{15}\sqrt{T_\pi}+D_{16}T_{\rm lab}^{D_{17}})$$

with constants D_i given in Table IV.

The negatively charged pion spectral distribution for the range 0.3–2 GeV is represented by the following equations:

$$F_2=G_1T_\pi^{G_2}+G_3T_{\rm lab}^{G_4},$$

$$F_1=\exp\left(G_5+\frac{G_6}{\sqrt{T_{\rm lab}}}+G_7T_\pi^{G_8}+G_9T_\pi^{G_{10}}\right), \tag{27}$$

$$\left(\frac{d\sigma}{dE}\right)_{\rm lab}=T_\pi^{G_{11}}\left(G_{12}\frac{F_1}{F_2}+G_{13}\exp\left(G_{14}\sqrt{T_\pi}\right)\right),$$

with constants G_i given in Table V.

The negatively charged pion spectral distribution for the range 2–50 GeV is represented by the following equations:

$$F_2=H_1T_\pi^{H_2}+H_3T_{\rm lab}^{H_4},$$

$$F_1=\exp\left(H_5+\frac{H_6}{\sqrt{T_{\rm lab}}}+H_7T_\pi^{H_8}+H_9T_\pi^{H_{10}}\right), \tag{28}$$

$$\left(\frac{d\sigma}{dE}\right)_{\rm lab}=H_{11}T_\pi^{H_{12}}\frac{F_1}{F_2}+H_{13}T_\pi^{H_{14}}\exp(H_{15}\sqrt{T_\pi}+H_{16}T_{\rm lab}^{H_{17}}),$$

with constants H_i given in Table VI.

Total inclusive cross sections are represented by the following equations:

TABLE V. Constants for Eq. (27).

$G_1=1.06\times10^{-9}$	$G_6=-1.5$	$G_{11}=0.25$
$G_2=-2.8$	$G_7=-30.5$	$G_{12}=2.5\times10^{6}$
$G_3=3.7\times10^{-8}$	$G_8=0.0938$	$G_{13}=7.96$
$G_4=-1.89$	$G_9=-24.6$	$G_{14}=-49.5$
$G_5=22.3$	$G_{10}=0.0313$	

TABLE VI. Constants for Eq. (28).

$H_1=2.39\times10^{-10}$	$H_7=-31.3$	$H_{13}=60322$
$H_2=-2.8$	$H_8=0.0938$	$H_{14}=1.1$
$H_3=1.14\times10^{-8}$	$H_9=-24.9$	$H_{15}=-65.9$
$H_4=-2.3$	$H_{10}=0.0313$	$H_{16}=-9.39$
$H_5=22.3$	$H_{11}=2.5\times10^{6}$	$H_{17}=-1.25$
$H_6=-2.23$	$H_{12}=0.25$	

$$\sigma_{\pi}0=\left(0.007+0.1\frac{\ln(T_{\rm lab})}{T_{\rm lab}}+\frac{0.3}{T_{\rm lab}^2}\right)^{-1}, \tag{29}$$

$$\sigma_{\pi^+}=\left(0.00717+0.0652\frac{\ln(T_{\rm lab})}{T_{\rm lab}}+\frac{0.162}{T_{\rm lab}^2}\right)^{-1} \tag{30}$$

$$\sigma_{\pi^-}=\left(0.00456+\frac{0.0846}{T_{\rm lab}^{0.5}}+\frac{0.577}{T_{\rm lab}^{1.5}}\right)^{-1}. \tag{31}$$

For neutral pions, spectral distributions and total cross sections that were based on our own parametrization given in Eq. (7) were also developed. The formula for the spectral distribution was not divided into two regions, and it is much simpler than the previous formulas

$$\left(\frac{d\sigma}{dE}\right)_{\rm lab}=\exp\left(K_1+\frac{K_2}{T_{\rm lab}^{0.4}}+\frac{K_3}{T_\pi^{0.2}}+\frac{K_4}{T_\pi^{0.4}}\right), \tag{32}$$

where $K_1=-5.8$, $K_2=-1.82$, $K_3=13.5$, and $K_4=-4.5$.

Because Eq. (7) and Stephens LIDCS parametrization integrate to nearly the same total cross section (see Fig. 4), separate total cross section parametrizations are not necessary [i.e., use Eq. (29)].

C. Discussion of figures

As discussed previously, Figs. 1–3 show a comparison of LIDCS parametrizations for π^0 production of Carey *et al.* [Eq. (5)] [15], Stephens and Badhwar [Eq. (6)] [20], and Eq. (7) plotted with data from [14–20]. The figures are graphs of cross section plotted against transverse momentum ($p_\perp$) for various values of c.m. energy $E_{\rm c.m.}$ and c.m. scattering angle (θ^*). Figure 1 shows that the parametrization of Carey *et al.* is not an adequate representation of the data. Figures 2 and 3 show that the parametrization of Stephens and Badhwar fails for high transverse momentum by severely underpredicting the cross section.

Figure 4 shows numerically integrated LIDCS parametrizations of Stephens and Badhwar [Eq. (6)] [20], of Carey *et al.* [Eq. (5)] [15], and of Eq. (7) (referred to as Kruger) for π^0 production plotted with a parametrization of the integrated formulas of Stephens and Badhwar referred to as Stephens-total-param [Eq. (29)]. Three data points from Whitmore [24] show that Carey's parametrization does not integrate to the correct values and that the rest are quite accurate (see [20] for more detail).

Figure 5 shows π^0 spectral distribution parametrizations given by Eqs. (23) and (24) plotted with LIDCS parametri-

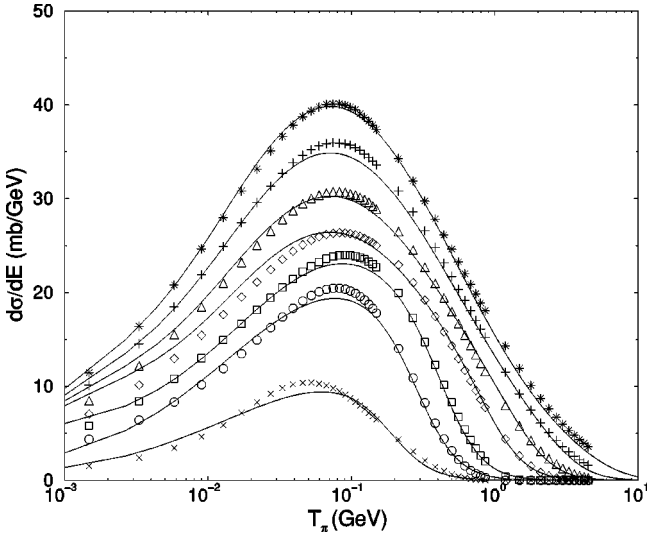

FIG. 5. π^0 spectral distribution parametrizations of Eqs. (23) and (24) (solid lines) plotted with LIDCS parametrization of Stephens and Badhwar [Eq. (6)] [20] numerically integrated at lab kinetic energies of 0.5, 1.0, 1.9, 5.0, 9.5, 20, and 50 GeV, listed in order of increasing cross section (symbols).

zation of Stephens and Badhwar [Eq. (6)] [20] numerically integrated at several lab kinetic energies. Figure 6 shows π^0 spectral distribution parametrizations given by Eq. (32) plotted with the numerical integration of Eq. (7). The shapes of the two spectral distributions look quite different even though both original LIDCS formula have a fit similar to the data at low $p_\perp$ where the cross section is the greatest, and both integrate to the same total cross section. This implies that the available data are not sufficient to tightly constrain the shape of the spectral distribution.

As discussed previously, Figs. 7–12 show π^+ and π^- LIDCS parametrizations of Alper *et al.* [Eq. (13)] [25],

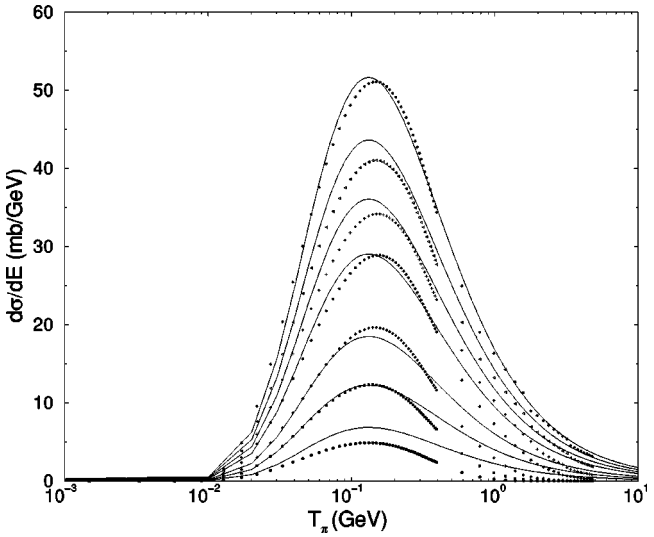

FIG. 6. π^0 spectral distribution parametrization of Eq. (32) (solid lines) plotted with Eq. (7) numerically integrated at lab kinetic energies of 0.5, 1.0, 1.9, 5.0, 9.5, 20, and 50 GeV, listed in order of increasing cross section (symbols).

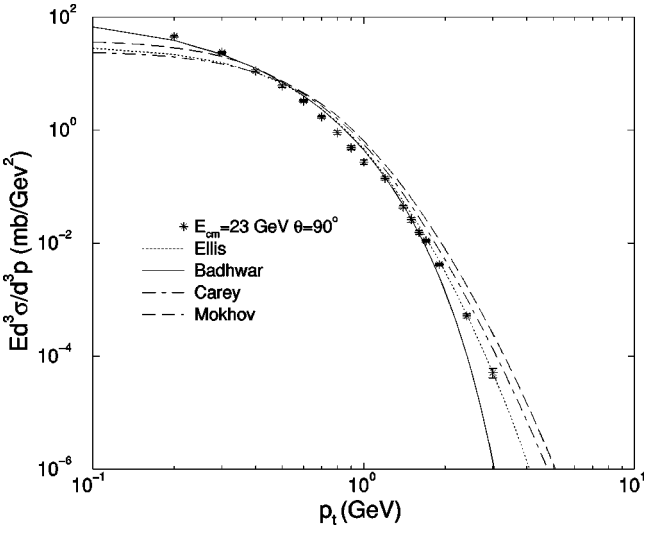

FIG. 7. π^- production parametrizations of Ellis and Stroynowski [Eq. (15)] [22], Badhwar *et al.* [Eq. (16)] [31], Carey *et al.* [Eq. (14)] [30], and of Mokhov and Striganov [Eq. (17)] [32] plotted with LIDCS data from [25]. LIDCS is plotted against transverse momentum for c.m. energy $E_{\text{c.m.}}=23$ GeV and pion c.m. scattering angle $\theta^*=90°$.

Badhwar *et al.* [Eq. (16)] [31], Ellis and Stroynowski [Eq. (15)] [22], Carey *et al.* [Eq. (14)] [30], and Mokhov and Striganov [Eq. (17)] [32], and LIDCS data from [16,25] plotted against transverse momentum ($p_t \equiv p_\perp$) for different values of c.m. energy $E_{\text{c.m.}}$, but all at $\theta^*=90°$. These graphs show that the parametrizations of Badhwar best fit the data, but underpredict the cross section for large transverse momentum.

Figure 13 shows the numerically integrated LIDCS parametrizations of Badhwar *et al.* [Eq. (16)] [31], and of Carey *et al.* [Eq. (14)] [30] for π^+ and π^- plotted with parametrizations of the integrated formulas of Badhwar referred to as present work [Eqs. (30) and (31)]. Three data

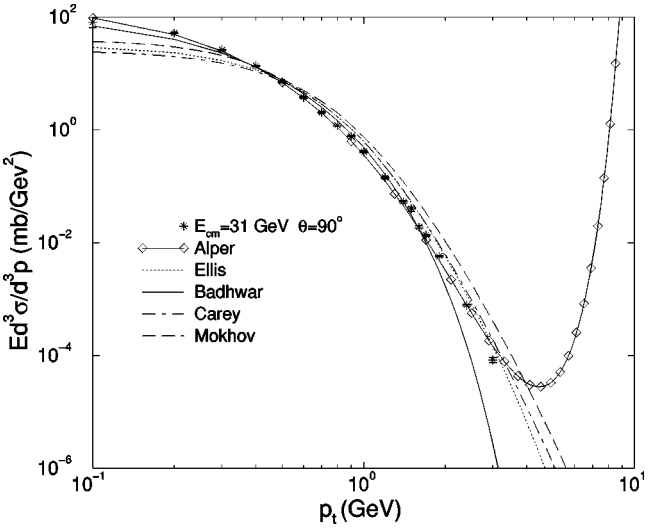

FIG. 8. π^- production. Same as Fig. 7 except $E_{\text{c.m.}}=31$ GeV, and the parametrization of Alper *et al.* [Eq. (13)] [25] is included.

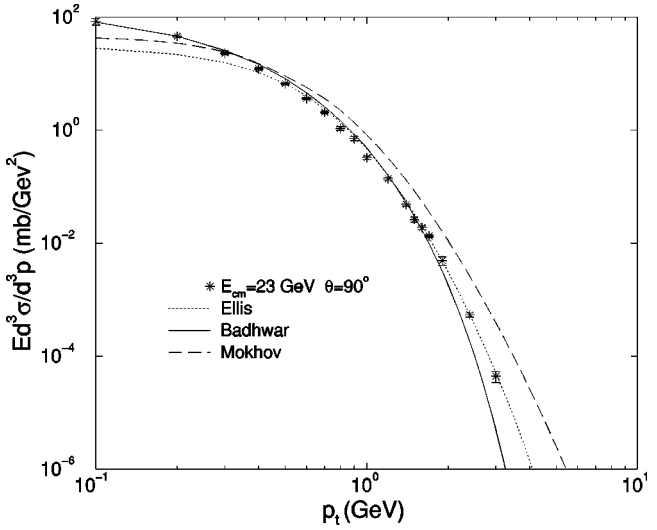

FIG. 9. π^+ production parametrizations of Ellis and Stroynowski [Eq. (15)] [22], Badhwar *et al.* [Eq. (16)] [31], and of Mokhov and Striganov [Eq. (17)] [32] plotted with LIDCS data from [25]. LIDCS is plotted against transverse momentum for c.m. energy $E_{\text{c.m.}}=23$ GeV and pion c.m. scattering angle $\theta^*=90°$.

points from Whitmore *et al.* [24] show that Carey's parametrization does not integrate to the correct values and that Badhwar's formula is accurate. The figures also show that the parametrization fits the numerically integrated formulas very well.

Figures 14 and 15 show π^- and π^+ spectral distribution parametrizations plotted with LIDCS parametrization of Badhwar *et al.* [Eq. (16)] [31] numerically integrated. The plot is of cross section $(d\sigma/dE)$ plotted against the kinetic energy of the produced pion T_π at several values for the lab kinetic energies of the colliding proton. The graphs clearly show that the spectral distribution parametrizations have excellent fits to the integrated LIDCS parametrizations.

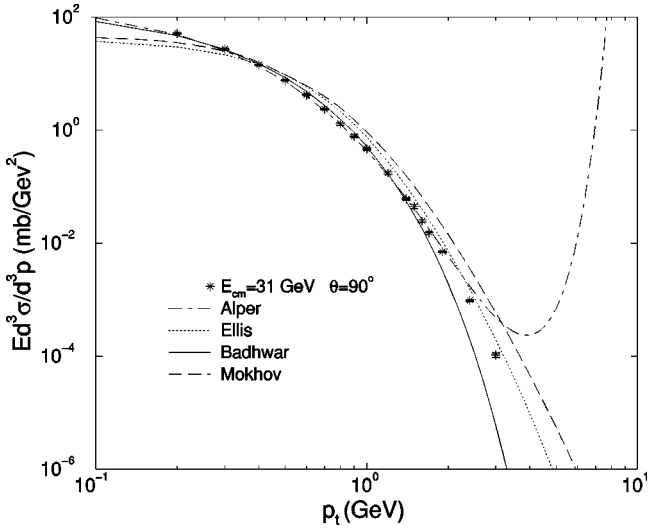

FIG. 10. π^+ production. Same as Fig. 9 except $E_{\text{c.m.}}=31$ GeV, and the parametrization of Alper *et al.* [Eq. (13)] [25] is included.

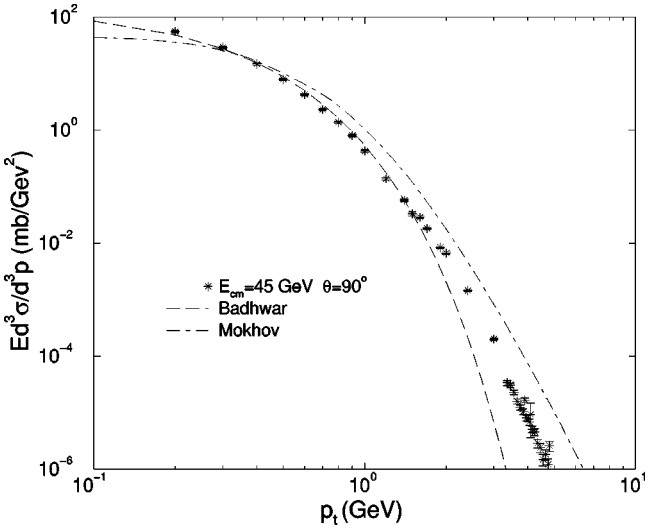

FIG. 11. π^+ production. Same as Fig. 9 except the data are from [16,25] for $E_{\text{c.m.}}=45.0$ and 44.8 GeV, and the parametrization of Ellis and Stroynowski [Eq. (15)] [22] is excluded. Parametrizations are plotted at $E_{\text{c.m.}}=45.0$ GeV.

IV. SUMMARY AND CONCLUSIONS

This paper presents parametrizations of cross sections for inclusive pion production in proton-proton collisions. The cross sections of interest are LIDCS, lab frame spectral distributions, and total cross sections. For neutral pions the parametrization of Stephens and Badhwar [20] [Eq. (6)] fit the data well for low values of $p_\perp$, but overpredicted the cross section by many orders of magnitude at high $p_\perp$ values. Because of this inaccuracy, Eq. (7) was developed. The final form of our resultant parametrization for the neutral pion invariant cross section in proton-proton collisions is Eq. (7) with $D(p_\perp,\sqrt{s},\theta^*)$ given in Eq. (11), $F(p_\perp,\sqrt{s})$ given in Eq. (8), and $G(q,p_\perp)$ given in Eq. (9). This formula is as

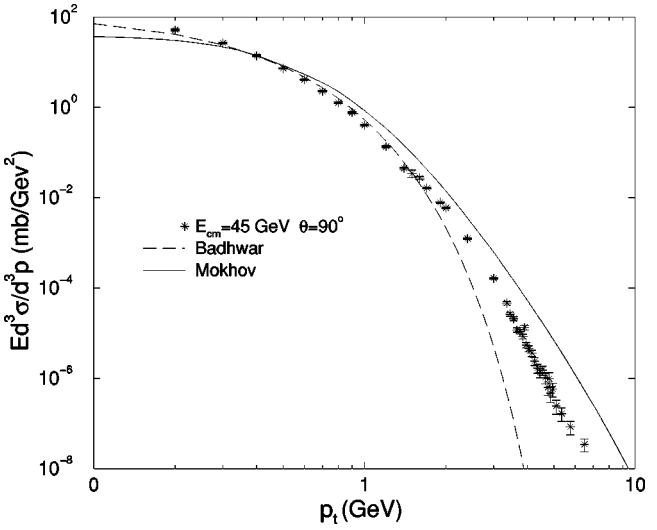

FIG. 12. π^- production. Same as Fig. 7 except the data are from [16,25] for $E_{\text{c.m.}}=45.0$ and 44.8 GeV, and some of the parametrizations are excluded. Parametrizations are plotted at $E_{\text{c.m.}}=45.0$ GeV.

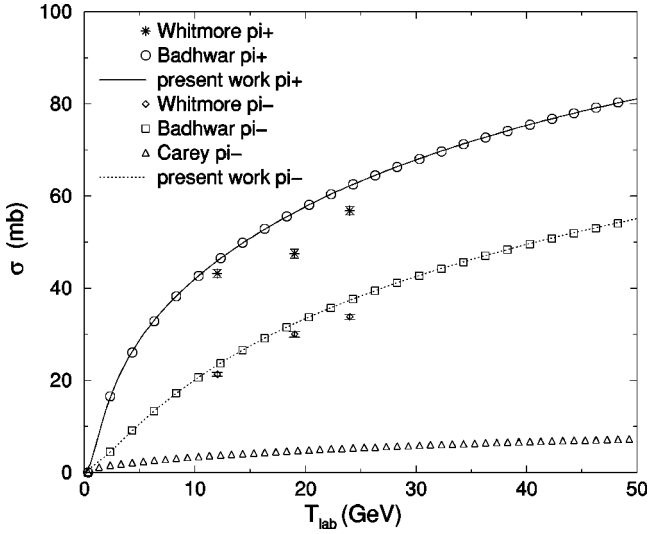

FIG. 13. Parametrizations of total $\pi^{\pm}$ production cross section (present work) [Eqs. (30) and (31)] plotted with numerically integrated LIDCS parametrizations of Badhwar *et al.* [Eq. (16)] [31] (circles and squares) and Carey *et al.* [Eq. (14)] [30] (triangles). Six data points are included for comparison (data are from Whitmore [24]).

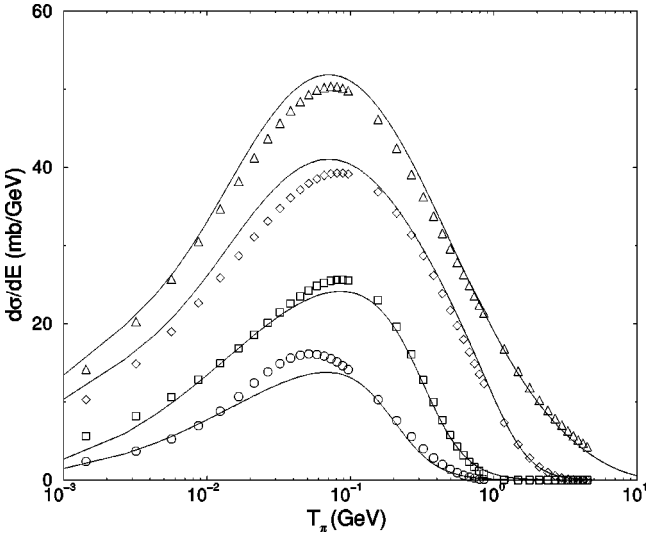

FIG. 15. π^{+} spectral distribution parametrizations [Eqs. (25) and (26)] (solid lines) plotted with LIDCS parametrization of Badhwar *et al.* [Eq. (16)] [31] (symbols) numerically integrated at lab kinetic energies of 0.5, 1.1, 5.0, and 50 GeV, listed in order of increasing cross section.

accurate as that of Stephens and Badhwar [20] at low $p_{\perp}$ values, but is much more accurate at high $p_{\perp}$ values. For charged pions the formulas of Badhwar *et al.* [Eq. (16)] [31] were found to best represent the data except at high $p_{\perp}$ values. These formulas were used in the development of spectral distributions and total cross sections because they are the most accurate at low $p_{\perp}$ where the cross section is the greatest.

The data for lab frame spectral distributions and total cross sections is scarce, so parametrizations for these quantities were developed using the above LIDCS formulas. These formulas were numerically integrated, resulting in discrete numerical ''data'' points for these other cross sections. The accuracy of the representations of lab frame spectral distributions and total cross sections is, therefore, limited to the accuracy of the original LIDCS. The numerical ''data'' were then parametrized so that closed form expressions [Eqs. (23)–(32)] could be obtained. As a check on the accuracy, the total cross section numerical ''data'' were compared to experimental data. They were found to agree quite well, but when the numerical ''data'' for the spectral distributions for the formulas for π^{0} production [Eqs. (23), (24) and (32)] are compared (i.e., compare Fig. 5 to Fig. 6), they are found to disagree. Since both original LIDCS formulas fit the data well at low $p_{\perp}$ where the cross section is greatest, and both formulas integrate to the correct total cross section, the available data must not be sufficient to uniquely determine the global behavior of the LIDCS. The data for charged pion production is much more limited than the data for neutral pion production, so the same problem exists for charged pions.

To more accurately determine the cross sections for space radiation applications, measurements of the spectral distribution at lower energies (for example, proton lab kinetic energies 3 and 8 GeV, and pion lab kinetic energies of 0.01, 0.1, and 1 GeV) would need to be taken. These measurements would put a much tighter constraint on the global properties of the LIDCS, and the spectral distribution parametrizations could also be made more accurate.

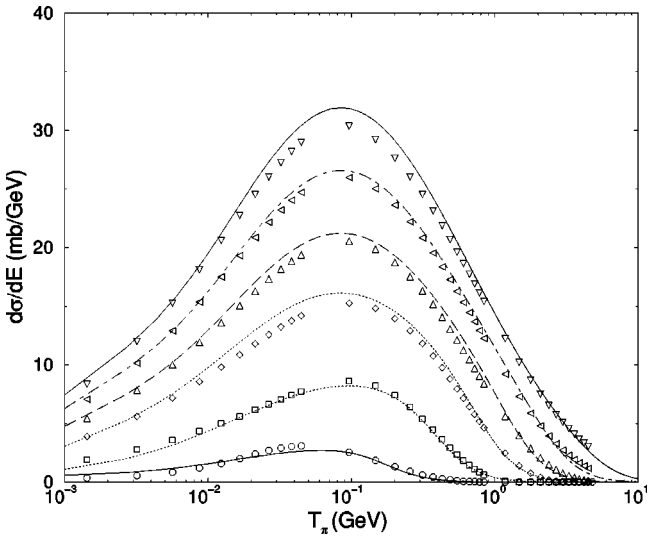

FIG. 14. π^{-} spectral distribution parametrizations [Eqs. (27) and (28)] (solid lines) plotted with LIDCS parametrization of Badhwar *et al.* [Eq. (16)] [31] (symbols) numerically integrated at lab kinetic energies of 0.5, 1.9, 5.0, 9.5, 20, and 50 GeV, listed in order of increasing cross section.

ACKNOWLEDGMENTS

The authors would like to thank Sean Ahern and Alfred Tang for their help on the project. S.R.B. was supported by the Wisconsin Space Grant Consortium, NASA Grant No.

NCC-1-260, and the NASA Graduate Student Researchers Program through Grant No. NGT-52217. A.T.K. and M.N. were supported by the Wisconsin Space Grant Consortium, NASA Grant No. NCC-1-260, and NSF Grant No. PHY-9507740. J.W.N. and S.R.S. were supported by NASA Grant Nos. NCC-1-260 and NCC-1-354.

APPENDIX: SYNOPSIS OF DATA TRANSFORMATIONS

The data that were used in the comparison of different parametrizations were given in terms of several different kinematic variables. Some of the LIDCS data were transformed so that all data would be expressed in terms of the same variables: $p_\perp$, θ^*, and $E_{\text{c.m.}}=\sqrt{s}$. The following is a synopsis of the transformations that were performed for the data plotted in the figures.

The data from Carey *et al.* [15] were listed for different values of P_p, $p_\perp$, and θ. $\sqrt{s}$, $p_\perp$, and θ were used by Eggert *et al.* Stephens and Badhwar [20] used photon production data from Fidecaro *et al.* [14] to derive pion production cross sections. The variables T_{lab}, θ, and p were used by Stephens. $\sqrt{s}$, $p_\perp$, and the longitudinal rapidity y were used by Alper *et al.* [25], but only data with $y=0$ was used in the figures. When $y=0$ then $\theta^*=90°$.

The necessary transformations are as follows:

$$p_\perp = p \sin\theta, \tag{A1}$$

T_{lab}, P_p, and θ can be transformed into $\sqrt{s}$ and θ^* by using the following Lorentz transformations to change to the c.m. frame. First express T_{lab} and P_p as total lab energy E

$$E = T_{\text{lab}} + m_p = \sqrt{P_p^2 + m_p^2}. \tag{A2}$$

Now perform the following Lorentz transformations:

$$E_{\text{cm}} = -\gamma v p \cos\theta + \gamma E, \tag{A3}$$

$$\theta^* = \tan^{-1}\left(\frac{p \sin\theta}{\gamma p \cos\theta - \gamma v E}\right), \tag{A4}$$

where

$$\gamma = \frac{T_{\text{lab}} + 2m_p}{\sqrt{s}}, \tag{A5}$$

$$v = \sqrt{1-\gamma^{-2}}. \tag{A6}$$

[1] R. Fernow, *Introduction to Experimental Particle Physics* (Cambridge University Press, New York, 1986); K. Kleinknecht, *Detectors for Particle Radiation*, 2nd ed. (Cambridge University Press, New York, 1998).
[2] M. V. S. Rao and B. V. Sreekantan, *Extensive Air Showers* (World Scientific, Singapore, 1998).
[3] T. K. Gaisser, *Cosmic Rays and Particle Physics* (Cambridge University Press, New York, 1990).
[4] P. Sokolsky, *Introduction to Ultrahigh Energy Cosmic Ray Physics* (Addison-Wesley, Redwood City, CA, 1989).
[5] J. W. Wilson *et al.*, Transport Methods and Interactions for Space Radiations, NASA Reference Publication No. 1257 (1991).
[6] J. L. Shinn *et al.*, IEEE Trans. Nucl. Sci. **45**, 2711 (1998).
[7] M. S. Longair, *High Energy Astrophysics*, 2nd ed. (Cambridge University Press, New York, 1992), Vol. 2.
[8] C. D. Dermer, Astrophys. J. **307**, 47 (1986); Astron. Astrophys. **157**, 223 (1986).
[9] F. W. Stecker, C. Done, M. H. Salmon, and P. Sommers, Phys. Rev. Lett. **66**, 2697 (1991); **69**, 2738 (1992).
[10] R. J. Protheroe, Nucl. Phys. B (Proc. Suppl.) **43**, 229 (1995).
[11] R. Mahadevan, R. Narayan, and J. Krolik, Astrophys. J. **486**, 268 (1997).
[12] E. Bycklng and K. Kajantie, *Particle Kinematics* (Wiley, New York, 1973).
[13] F. W. Busser *et al.*, Phys. Lett. **46B**, 471 (1973).
[14] M. Fidecaro *et al.*, Nuovo Cimento **24**, 73 (1962).
[15] D. C. Carey *et al.*, Phys. Rev. D **14**, 1196 (1976).
[16] F. W. Busser *et al.*, Nucl. Phys. **B106**, 1 (1976).
[17] K. Eggert *et al.*, Nucl. Phys. **B98**, 49 (1975).
[18] D. Lloyd Owen *et al.*, Phys. Rev. Lett. **45**, 89 (1980); the complete set of data is not given in the paper, but is listed at http://durpdg.dur.ac.uk/scripts/tabkum.csh/TABLE/3770/999/1/1
[19] A. L. S. Angelis *et al.*, Phys. Lett. B **185**, 213 (1987).
[20] S. A. Stephens and G. D. Badhwar, Astrophys. Space Sci. **76**, 213 (1981).
[21] R. Albrecht *et al.*, Eur. Phys. J. C **5**, 255 (1998).
[22] S. D. Ellis and R. Stroynowski, Rev. Mod. Phys. **49**, 753 (1977).
[23] D. C. Carey *et al.*, Phys. Rev. Lett. **33**, 327 (1974).
[24] J. Whitmore, Phys. Rep., Phys. Lett. **10C**, 273 (1974).
[25] B. Alper *et al.*, Nucl. Phys. **B100**, 237 (1975).
[26] Manufactured by SPSS Inc., Table Curve 3D v3, AISN Software Inc. (copyright 1997).
[27] P. Capiluppi *et al.*, Nucl. Phys. **B79**, 189 (1974).
[28] P. Capiluppi, G. Giacomelli, A. M. Rossi, G. Vannini, and A. Bussiere, Nucl. Phys. **B70**, 1 (1974).
[29] M. G. Albrow *et al.*, Phys. Lett. **42B**, 279 (1972).
[30] D. C. Carey *et al.*, Phys. Rev. Lett. **33**, 330 (1974).
[31] G. D. Badhwar, S. A. Stephens, and R. L. Golden, Phys. Rev. D **15**, 820 (1977).
[32] N. V. Mokhov and S. I. Striganov, CP435, Workshop on the Front End of a Muon Collider, 1998, pp. 453–459.